Combining density-functional calculations with kinetic models: NO/Rh(111)

Combining density-functional calculations with kinetic models: NO/Rh(111)

C. G. M. Hermse,[a] F. Frechard, A. P. van Bavel, J. J. Lukkien, J. W. Niemantsverdriet, R. A. van Santen, and A. P. J. Jansen[b]
Schuit Institute of Catalysis, T/SKA, Eindhoven University of Technology, P. O. Box 513, 5600 MB Eindhoven, The Netherlands

(Received 18 November 2002; accepted 21 January 2003)

We present a dynamic Monte-Carlo model involving lateral interactions and different adsorption sites (top, fcc and hcp). Using this model in combination with kinetic parameters from UHV experiments and lateral interactions derived from DFT calculations we have reproduced the ordering behavior of NO on Rh(111) during adsorption and the temperature programmed desorption (TPD) of NO from Rh(111) under UHV conditions. The formation of c(4×2)-2NO domains at 0.50 ML coverage is shown to depend strongly on the next-next-nearest-neighbor repulsion between the NO adsorbates in our model. The formation of the (2×2)-3NO structure at higher coverage follows from the avoidance of the strong next-nearest-neighbor repulsion in favor of the occupation of the top sites. A single-site model was able to reproduce the experimental TPD, but the lateral interactions were at odds with the values of the DFT calculations. A three-site model resolved this problem. It was found that all NO dissociates during TPD for initial coverages of NO below 0.20 ML. The nitrogen atoms recombine at higher temperatures. For NO coverages larger than 0.20 ML, 0.20 ML NO dissociates while the rest desorbs. This is due to a lack of accessible sites on the surface, i.e., sites where a molecule can bind without experiencing large repulsions with neighboring adsorbates. For NO coverages above 0.20 ML, the dissociation of NO causes a segregation into separate NO and N+O islands. The dissociation causes the surface to be filled with adsorbates, and the adsorbates are therefore pushed closer together. NO on one hand can easily be compressed into islands of 0.50 ML coverage, because there is no large next-next-nearest-neighbor repulsion. N+O on the other hand form islands with a lower coverage (0.30–0.35 ML) due to the considerable next-next-nearest-neighbor repulsion. Top bound NO (above 0.50 ML initial coverage) does not dissociate during TPD. It desorbs in a separate peak at 380 K. © *2003 American Institute of Physics.* [DOI: 10.1063/1.1560139]

I. INTRODUCTION

The ability of Rh to efficiently dissociate NO makes it the most suitable metal for the removal of nitrogen oxides from automotive exhaust gases in catalytic converters. The system of NO on Rh(111) has subsequently been extensively studied under UHV conditions. Adsorption of NO is molecular below 275 K, and two ordered structures can be formed depending on the temperature, one at around 0.50 ML, and one at close to 0.75 ML.[1,2] These structures have been deduced from LEED measurements. The structure at 0.50 ML is thought to consist of three types of domains which are rotated 120 degrees with respect to each other. The (2×2)-3NO saturation structure is only formed at temperatures above 225 K. At lower temperatures the saturation coverage decreases to 0.68 ML.[3] The configuration of the adlayer at these lower temperatures is still unclear. Similar ordered structures are also known for NO on Ni(111) and Ru(001).[4,5]

In TPD experiments, it was found that there are three distinct coverage regions displaying differing behavior.[6] Below 0.25 ML all NO dissociates between 275 and 325 K, indicating sufficient accessible sites on the surface. The N adatoms formed in the dissociation recombine in a second order peak between 450 and 650 K. The oxygen adatoms recombine at temperatures above 900 K. At intermediate coverages (between 0.25 and 0.50 ML), part of the NO is thought to dissociate (above 300 K), filling the empty available threefold sites on the surface. When all empty sites are filled, the dissociation is inhibited until the desorption of NO. Above 400 K, part of the remaining NO desorbs, while another part dissociates after all. Nitrogen gas is formed in two peaks, one of which coincides with the NO desorption peak, the other one is at higher temperatures. At coverages above 0.50 ML the top sites become occupied as well, resulting in an additional NO desorption peak at 380 K. Dissociation of NO is totally inhibited up to over 400 K, when the threefold bound NO starts desorbing. These different types of behavior are all related to the interactions between the adsorbates; because of the repulsion reactions can be suppressed or enhanced, while different sites may be occupied to prevent strong repulsion.

All these observations ask for a better view of the adsorbate distribution on the single crystal surface. In this article we introduce a three-site Monte-Carlo model with lateral interactions in order to get a deeper insight into how the adsorbates, NO, N and O in particular, are distributed on the catalytically active Rh(111) surface.

[a]Electronic mail: c.g.m.hermse@tue.nl
[b]Electronic mail: tgtatj@chem.tue.nl; www.catalysis.nl/theory

II. METHOD

A. Dynamic Monte-Carlo

We have simulated the reactions with Dynamic Monte-Carlo simulations.[7–9] The surface is represented by a lattice, with each point corresponding to a surface site. Every lattice point is labeled according to the type of site, and the type of adsorbate occupying the site. A lattice with labels for all its lattice points is called a configuration. This configuration can be transformed into another one by means of a reaction. The evolution of the system as a function of (real) time can be described by means of the chemical Master Equation, which can be derived from first principles:[10,11]

$$\frac{dP(c,t)}{dt}=\sum_{c'\neq c}[k_{cc'}P(c',t)-k_{c'c}P(c,t)]. \tag{1}$$

In this equation, $P(c,t)$ denotes the probability to find the system in configuration c at time t; $k_{c'c}$ is the transition probability per unit time of the reaction that transfers c into c'. This transition probability can be interpreted as a microscopic rate constant, which can be described by the Arrhenius equation:

$$k_{c'c}=\nu_{c'c}\exp\left(-\frac{E_{c'c}}{k_BT}\right), \tag{2}$$

where $E_{c'c}$ stands for the activation energy, and $\nu_{c'c}$ is the pre-exponential factor of the reaction that transforms c into c'. There are several families of algorithms to solve the Master Equation; we have used the discrete event simulation algorithm (DES).[7] This algorithm, also known as the first reaction method (FRM), can handle the time-dependent rate constants used in the TPD simulations. In the DES algorithm, a tentative time is calculated for every possible reaction. All reactions together with their tentative times are stored in an event list. The algorithm proceeds by repeatedly performing the following steps: select the reaction with minimal time from the event list, advance the system time to the time of this reaction, adjust the lattice according to the reaction, and update the event list.

B. Lateral interactions

Reactant or product states of a certain reaction are often (de-)stabilized by the presence of other adsorbates. Since the transition state usually has characteristics of both the reactant and the product state, it will also shift in energy. The activation barrier will therefore in general change in the presence of other adsorbates. Calculating transition states, and shifts in transition states due to co-adsorbates using DFT is quite laborious and involves many calculations. We have therefore estimated the influence of other adsorbates on the activation energy by means of the Brønsted-Polanyi relation[12–15] which holds provided that the energy changes are small ($\delta E < E^0_{\mathrm{act}}$) and the reaction mechanism does not change:

$$E'_{\mathrm{act}}=E^0_{\mathrm{act}}+\alpha\delta E, \tag{3}$$

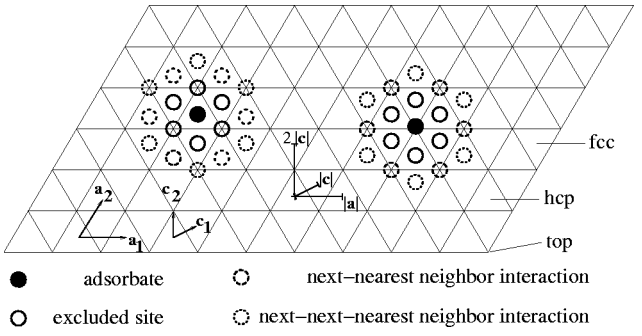

FIG. 1. Excluded sites and lateral interactions in the three-site model.

where E'_{act} (E^0_{act}) is the activation energy with (without) lateral interactions, α is the Brønsted-Polanyi coefficient ($\alpha \in [0,1]$) and δE is the change in reaction energy caused by lateral interactions,

$$\delta E=(E'_{\mathrm{prod}}-E'_{\mathrm{react}})-(E^0_{\mathrm{prod}}-E^0_{\mathrm{react}}), \tag{4}$$

where E'_{react} (E^0_{react}) equals the energy of the reactants with (without) lateral interactions and E'_{prod} (E^0_{prod}) equals the energy of the products with (without) lateral interactions. This can also be written as

$$\delta E=(E'_{\mathrm{prod}}-E^0_{\mathrm{prod}})-(E'_{\mathrm{react}}-E^0_{\mathrm{react}}). \tag{5}$$

If the interactions are assumed to be pairwise additive, we can write

$$E'_{\mathrm{react}}-E^0_{\mathrm{react}}=\sum_i \varphi_{react}(i), \tag{6}$$

and a similar expression for the products. The sum is over all pair interactions and $\varphi(i)$ is the corresponding energy. To calculate δE we only have to include terms that change.

The Brønsted-Polanyi coefficient α defines the type of transition state. If $\alpha=0$, there is an early barrier and the transition state shifts with the reactant state. Lateral interactions therefore do not influence the activation energy. If $\alpha=1$, there is a late barrier and the transition state shifts with the product state. In this case (and any other case in which $\alpha>0$) lateral interactions do influence the activation energy.

The difference of the activation energies of the forward and the backward reaction is always equal to the difference in energy between the reactant and the product state. At sufficiently high temperatures a correct Gibbs distribution will therefore be reached.

C. The reaction model

Our model consists of a lattice of top, fcc and hcp sites. These three sites form a regular grid (Fig. 1) with a spacing of $1/\sqrt{3}$ lattice vectors, where the grid unit cell vectors ($\mathbf{c_1}$ and $\mathbf{c_2}$) are at a 30 degree angle with the lattice vectors ($\mathbf{a_1}$ and $\mathbf{a_2}$) of the (111) surface. Every site is labeled t, f or h according to its type, with a prefix to indicate the type of adsorbate: NO, N, O or * (the last stands for an empty site).

Based on the results from the DFT calculations, which are presented in the Results and Discussion section, we have excluded the sites nearest to an adsorbate from occupation (at distance $|\mathbf{c}|$, see Fig. 1). Two other kinds of lateral inter-

TABLE I. Kinetic parameters for NO on Rh(111).

	ν (s^{-1})	E_{act} (kJ/mol)	Notes
NO Adsorption			
NO adsorption	0.01	—	Ref. 20
NO diffusion:			
threefold → threefold	10^9–10^{13}	22.5	This work
threefold → top	10^9–10^{13}	47	This work
top → threefold	10^9–10^{13}	0	This work
NO TPD/TPR			
Diffusion:			
NO, N and O	1000	—	
NO dissociation	10^{11}	65	Ref. 6
NO desorption:			
from top site	$10^{13.5}$	129	Ref. 6, adapted
from threefold site	$10^{13.5}$	133	Fitted
N_2 formation	10^{10}	120	Ref. 6

actions have been taken into account: one at the next-nearest-neighbor site (one lattice vector, $|\mathbf{a}|$ apart), the other one at the next-next-nearest-neighbor site ($2/\sqrt{3}$ lattice vector or 2 $|\mathbf{c}|$ apart).

We have included the following reactions:

$$*_{\text{threefold}} \rightleftarrows NO_{\text{threefold}} \tag{7}$$

$$*_{\text{top}} \rightleftarrows NO_{\text{top}} \tag{8}$$

$$NO_{\text{threefold}} + *_{\text{threefold}} \rightarrow N_{\text{threefold}} + O_{\text{threefold}} \tag{9}$$

$$2N_{\text{threefold}} \rightarrow 2*_{\text{threefold}} \tag{10}$$

and diffusion of NO, N and O:

$$NO_{\text{threefold}} + *_{\text{threefold}} \rightleftarrows *_{\text{threefold}} + NO_{\text{threefold}} \tag{11}$$

$$NO_{\text{threefold}} + *_{\text{top}} \rightleftarrows *_{\text{threefold}} + NO_{\text{top}} \tag{12}$$

$$N_{\text{threefold}} + *_{\text{threefold}} \rightleftarrows *_{\text{threefold}} + N_{\text{threefold}} \tag{13}$$

$$O_{\text{threefold}} + *_{\text{threefold}} \rightleftarrows *_{\text{threefold}} + O_{\text{threefold}}. \tag{14}$$

We did not include the bridge site in our model, despite the fact that it has an adsorption energy which lies between the values for the threefold and the top site. The reason for not including the bridge site stems from the observation by means of XPS[16] and EELS[1,17] that NO on Rh(111) occupies only two kinds of sites, which were later identified as top and threefold.[2,18] Probably the bridge sites do not allow for a favorable distribution of adsorbates avoiding lateral interactions, and are therefore not significantly occupied.

The kinetic parameters we have used are listed in Table I. Most have been adopted from Ref. 6. Diffusion was modeled with Arrhenius-type rate constants for the low-temperature adsorption simulations, with prefactors between 10^9 and 10^{13} s^{-1} and the activation energies derived from the differences in binding energies between top, bridge and threefold sites in the DFT calculations. For simplicity we have treated the threefold sites as equivalent in our DMC model, though a difference in binding energy of typically 10 kJ/mol was observed between fcc and hcp sites. Diffusion was not modeled with Arrhenius-type rate constants for the TPD/TPR simulations because it increases with several decades over the simulated temperature range. Instead, rate constants for diffusion were set to 1000 s^{-1}, modified by lateral interactions and differences in site adsorption energies:

$$k_{\text{threefold}\rightarrow\text{threefold}} = 1000\ s^{-1} \times e^{(\alpha \delta E)/RT} \tag{15}$$

$$k_{\text{threefold}\rightarrow\text{top}} = 1000\ s^{-1} \times e^{(\alpha'(\delta E) - 0.5\Delta E_b)/RT} \tag{16}$$

$$k_{\text{top}\rightarrow\text{threefold}} = 1000\ s^{-1} \times e^{((1-\alpha')(\delta E) + 0.5\Delta E_b)/RT}, \tag{17}$$

where δE equals the shift in energy due to lateral interactions as defined in Eq. (4), and ΔE_b is the difference in binding energy between the top and the threefold site. Tests with various prefactors have shown that the reduction of nitrogen diffusion only slightly lowers the rate of nitrogen formation. The reduction of other diffusion rates did not cause significantly differing behavior. So our modeling of the diffusion yields an adlayer at equilibrium without too much computer time spent on diffusion. The desorption of top bound NO is reasonably well-defined, since it occurs from an ordered structure (the (2×2)-3NO structure). Desorption of threefold NO on the other hand only happens when the surface is filled with N and O atoms. The measured activation energy of desorption is dependent on the lateral interactions with the N and O atoms present. The spatial distribution of these atoms is unknown; we have therefore not used the activation energy of desorption from threefold sites that has been reported in literature (Ref. 6), but fitted the value using the prefactor for top bound NO desorption. The oxygen atom formed in the dissociation reaction was deposited $2/\sqrt{3}$ lattice vectors away from the nitrogen, nitrogen formation was allowed at a distance of $3/\sqrt{3}$ lattice vectors. Precursor adsorption of NO[19] was not included in the model, since we are mainly interested in the ordering on the surface, and not in the adsorption process itself. Since oxygen formation only takes place above 900 K, it was also left out of the model. The grid sizes used were 132×132 for the adsorption simulations and 264×264 for the TPD/TPR simulations.

In view of the difference in energy between reactant and product we have taken desorption to be a late transition state (and therefore adsorption to be an early transition state), NO dissociation and N recombination to be late transition states ($\alpha = 1$), and diffusion to be a middle transition state ($\alpha = 0.5$).

A simpler model with only one type of site, which was described previously,[20,21] was also considered. This model consists of a lattice of threefold sites; one site per metal atom, so either fcc or hcp. A nearest-neighbor interaction has been taken into account. Note that the nearest-neighbor in this single-site model is the *next*-nearest-neighbor in the three-site model, one lattice vector or $|\mathbf{a}|$ apart. Reactions described in Eqs. (7), (9), (10), and diffusion of all species [Eqs. (11), (13), (14)] were included. The kinetic parameters used were the same as for the three-site model, except for the desorption of NO, for which the prefactor and activation energy were fitted to $10^{12.5}$ s^{-1} and 118 kJ/mol. Similar models but with fewer types of adsorbates were previously published by Honkala *et al.*, Stampfl *et al.* and Hansen *et al.*[22–24]

TABLE II. Adsorption energies on Rh(111). Energies are in kJ/mol relative to the molecular gas phase species (i.e., O_2 for O and N_2 for N).

Site	Coverage (ML)	NO	O	N
fcc	0.11	−245	−195	−23
	0.25	−230	−195	−11
hcp	0.11	−248	−189	−37
	0.25	−238	−185	−20
bridge	0.11	−224	−147	−17
	0.25	−218		
top	0.11	−187		
	0.25	−184		

TABLE III. Adsorption energies per adsorbate (averaged, kJ/mol) on Rh(111) for different ordered structures. The coverage is 0.50 ML unless otherwise stated. Energies are relative to the molecular gas phase species (i.e., O_2 for O and N_2 for N).

	NO hcp	O fcc	N hcp
p(2×1) rows	−212	−170	+20
	NO fcc+hcp	O fcc+hcp	N fcc+hcp
c(4×2) zig-zag	−232	−163	+6
(2×2) honeycomb	−233		
	NO fcc+hcp+top		
(2×2)-3NO 0.75ML	−208		

D. DFT

The VASP code[25,26] allows periodic DFT calculations (Perdew and Wang functional[27]) with a plane wave basis set and the ultrasoft pseudopotentials introduced by Vanderbilt[28] and generated by G. Kresse and J. Hafner.[29] The surfaces were modeled by a supercell containing a 5 layer slab and 13.5 Å of vacuum between the surfaces. For all the calculations the energy cut-off for the plane wave basis set was set to 400 eV as it corresponds to the value for which all the ultrasoft pseudopotentials are converged. The k-point sampling was done following the Monkhorst-Pack procedure, with $5\times5\times1$ grids for the (2×2) and c(4×2) cells and a $3\times3\times1$ grid for the (3×3) cell, Gaussian smearing ($\alpha=0.2$ eV) was applied to the electronics levels. Adsorption was done on both sides of the slab, with at least an inversion center (no spurious dipole-dipole interactions) and depending on the starting geometry additional symmetry operations were used. A complete geometry optimization was performed for each configuration. All the parameters (k-points, FFT grids, numerical approximations) were extensively tested and the energies are converged within 3 kJ/mol. Various coverages (0.11, 0.25, 0.50 and 0.75 ML) with different structures ((3×3), (2×2) and c(4×2)) were considered to determine the lateral interactions. Gas phase molecules (NO, O_2 and N_2) were calculated in the (3×3) cell, spin polarization was included for NO and O_2 but was disregarded for adsorption as calculations showed that the spin disappears upon adsorption.

III. RESULTS AND DISCUSSION

A. DFT results

Some lateral interactions could be extracted from the data presented in Ref. 30 but the data set was not sufficient for extrapolating a full set of pairwise lateral interactions for the three species (O, N and NO) adsorbed simultaneously. We have therefore done additional calculations, presented in Tables II–IV.

An important point in viewing these tables concerns the accuracy of the DFT calculations (i.e., the DFT functionals) with some systems and particularly for the adsorption of NO on metals. Microcalorimetry experiments have shown an overestimation of the calculated adsorption energies.[31] The absolute adsorption energies have therefore not been used as an estimate of the activation energy for desorption. Table II lists the adsorption energies at low coverages. A p(2×2) and a p(3×3) unit cell were used to get the 0.25 and 0.11 ML coverage. The difference in the adsorption energy for the two different coverages is small for the top and bridge site, while the difference is in general larger for adsorbates in the threefold sites. This is due to the way the Rh-atoms settle around the adsorbate. If the difference in adsorption energy is treated as a pairwise interaction, it amounts to less than 5 kJ/mol. Because of the large separation, and the many other interactions possible at closer range, these interactions were not taken into consideration in our DMC model. As the difference in adsorption energies between threefold and bridge sites is not large it is clear that diffusion of all listed adsorbates is fast.

Table III lists the adsorption energies for higher coverages. The listed structures were chosen in such a way that the interactions could be easily determined. If more structures and a least-squares fit are used for determining the lateral interactions, they remain essentially the same. The comparison of the values in Table III with the values in Table II yield the pairwise lateral interactions for each adsorbate *i*:

$$\varphi(i)=(E_{\text{ads,alone}}-E_{\text{ads,coadsorbed}})/n, \tag{18}$$

where *n* is the number of pairwise interactions per adsorbate in the coadsorbed structure. The pairwise additivity of the interactions is a good approximation provided that the adsorption geometry does not change much (due to lateral in-

TABLE IV. Summed adsorption energies (kJ/mol) per unit cell on Rh(111) for different ordered coadsorbed structures at 0.50 ML coverage. Each unit cell contains two (different) adsorbates. Energies are relative to the molecular gas phase species (i.e., O_2 for O and N_2 for N).

	NO fcc+O fcc	NO hcp+N hcp	O fcc+N fcc
(2×2) rows	−223	−211	−107
	NO hcp+O fcc	NO fcc+N hcp	O fcc+N hcp
(2x$\sqrt{3}$) zig-zag	−403	−218	−165
	NO top+O fcc	NO top+N hcp	
(2×2) honeycomb	−363	−205	

TABLE V. Lateral interactions for NO on Rh(111) (kJ/mol) at 1 $d_{\text{Rh-Rh}}$ (next-nearest neighbor) and $2/\sqrt{3}\ d_{\text{Rh-Rh}}$ (next-next-nearest neighbor); three-site model using DFT-results. Since the interactions are pairwise, the lower left part of the table is identical to the upper right part. We have therefore only reported the lower left part.

	NO threefold			
NO threefold	26, 0	NO top		
NO top	—, 5	0, —	N threefold	
N threefold	24, 16	—, 0	40, 22	O threefold
O threefold	101 , 15	—, 7	46, 25	26, 26

teractions) and the interaction energy is much smaller than the adsorption energy ($\varphi \ll E_{\text{ads}}$). For example, to calculate the next-nearest-neighbor interaction for O, we take the difference of the p(2×2) fcc site adsorption energy (−195 kJ/mol) and the p(2×1) adsorption energy (−170 kJ/mol), and divide that by the number of pair interactions at next-nearest-neighbor distance in the p(2×1) structure (1). The result, 26 kJ/mol, is listed in Table V. Similarly for the next-next nearest-neighbor interaction of O we take the difference between the average p(2×2) adsorption energy of fcc and hcp bound O (−190 kJ/mol) and the c(4×2) zig-zag adsorption energy (−163 kJ/mol), divided by one. Interactions between different kinds of adsorbates were also calculated, the ordered structures used in our calculations are shown in Fig. 2, the summed adsorption energies are listed in Table IV.

The general trend in the interactions for threefold site bound adsorbates is that the next-nearest-neighbor interaction is strongly repulsive (anywhere between 25 and 100 kJ/mol) due to the bonding of both adsorbates to the same Rh-surface atoms. The next-next-nearest interaction is much smaller (0 to 25 kJ/mol). The interaction between top-bound NO and other, threefold bound, adsorbates is weakly repulsive. Because of the large repulsion at close distance we have excluded the occupation of nearest-neighbor sites ($1/\sqrt{3}$ lattice vectors separated), and applied the lateral interactions for adsorbates at next- and next-next-nearest-neighbors (1 and $2/\sqrt{3}$ lattice vectors separated) in our Dynamic Monte-Carlo model.

The activation energy for the NO dissociation ((2×2) structure) on a perfect Rh(111) surface has been previously

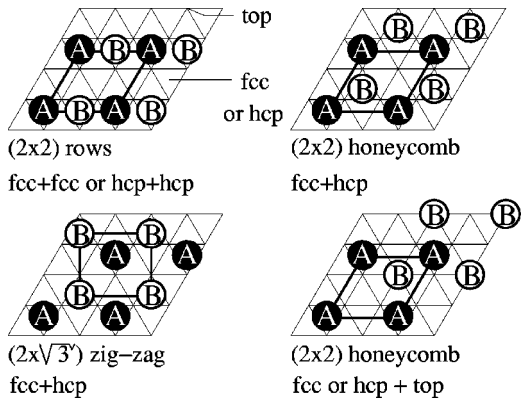

FIG. 2. Coadsorption structures simulated using DFT.

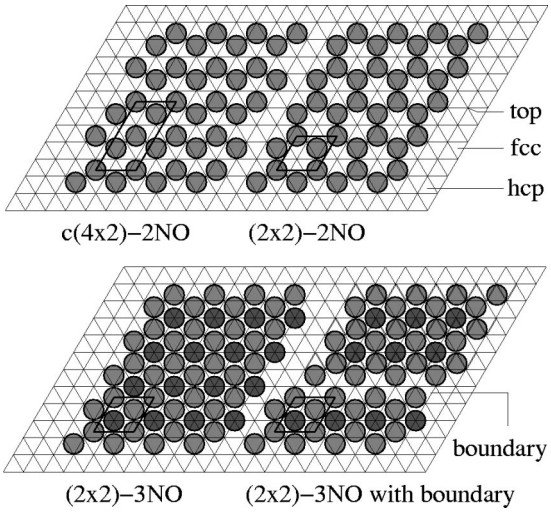

FIG. 3. Ordered structures of NO on Rh(111).

determined.[32] A calculation with our system gives almost the same activation energy of 157 kJ/mol which is what we expected as the models are similar and the method identical. This activation energy is much higher than the experimental results, which can be explained by a different dissociation mechanism, most likely at steps in the surface.

B. Ordering of the NO adlayer

We have started by simulating the adsorption of NO at low temperatures (150–225 K). At these temperatures NO adsorbs molecularly; dissociation only starts above 275 K.[6] In our simulations of the adsorption of NO, the threefold sites are occupied first, since they are energetically more favorable. Above 0.40 ML adsorbates start forming patches of ordered structures. Two ordered structures (Fig. 3) are encountered over the entire simulated temperature range (125–225 K), first the experimentally found c(4×2)-2NO structure, in which each adsorbed NO has two nearest-neighbors. The other ordered structure is a (2×2)-2NO structure, with one adsorbate fcc, one adsorbate hcp, arranged in a honeycomb-lattice. Every adsorbate has three nearest-neighbors. The c(4×2)-2NO structure can be transformed into the (2×2)-2NO structure by shifting each second zig-zag row by one lattice vector. The difference in adsorption energy between the two structures equals half a next-next-nearest-neighbor NO–NO interaction per adsorbate; each NO having 1 interaction in the c(4×2)-2NO structure, and 1.5 in the (2×2)-2NO structure. Both structures are therefore equal in energy when the DFT-based next-next-nearest-neighbor NO–NO interaction of 0 kJ/mol is used. Since this value has a non-negligible error margin, we have investigated interactions between 0 and 4 kJ/mol repulsive. The (2×2)-2NO structure dominates at 0.50 ML in the absence of a next-next-nearest-neighbor lateral interaction, resulting in many small ordered islands of 50–200 adsorbates (Fig. 4). In the case of a small repulsive next-next-nearest-neighbor lateral interaction, the c(4×2)-2NO structure dominates, with island sizes of 50–200 adsorbates for an interaction of 2 kJ/mol, and up to over 1000 adsorbates for an interaction of

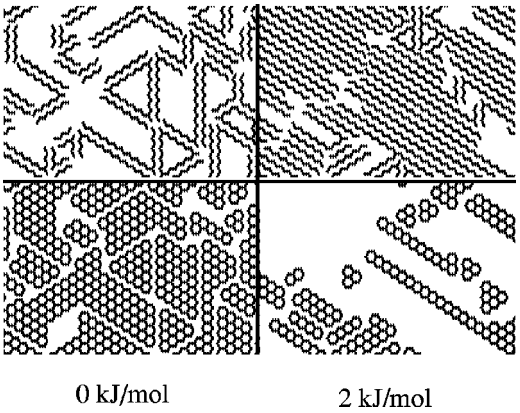

FIG. 4. Adsorbate distribution after adsorption at 225 K and 0.50 ML for a next-next-nearest-neighbor NO–NO repulsion of 0 (left) and 2 kJ/mol (right). Since the ordering is hard to recognize from the original output, two separate images are displayed for each result, with the characteristic zig-zag lines of the c(4×2)-2NO structure (upper panels) or the hexagons of the (2×2)-2NO structure (lower panels) emphasized. Snapshot of 55×35 lattice vectors.

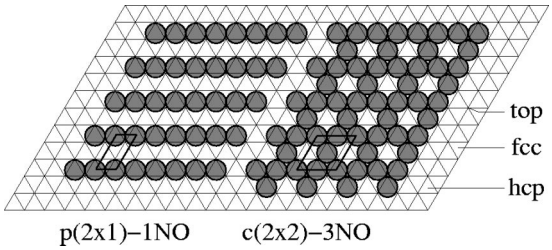

FIG. 5. Minimum energy adsorption structures at 0.50 ML (left) and 0.75 ML (right) in the single-site model.

4 kJ/mol (not shown). The basic cause for ordering at this coverage is the avoidance of occupying next-nearest-neighbor sites and/or low adsorption energy (i.e., top) sites.

If the coverage is gradually increased to values above 0.50 ML, the NO molecules are forced to either adsorb close to each other (next-nearest-neighbor position, resulting in a 26 kJ/mol repulsion per interaction) or to adsorb on another kind of sites, the top sites (47 kJ/mol less stable). Experimentally the top sites are found to become occupied. The top sites have a lower adsorption energy, but a structure can be formed with small lateral interactions and a high coverage of 0.75 ML. The adsorbates in this structure form a hexagonal packing, which is as dense as can be without next-nearest-neighbor interactions. In our model, this (2×2)-3NO structure is also found. The islands are separated by c(4×2)-2NO-like domains (2 zig-zag lines, then another (2×2)-3NO domain, Fig. 3). For a zero next-next-nearest-neighbor lateral interaction, the (2×2)-3NO structure is easily formed at high diffusion and at 225 K. For lower temperatures, the structure is formed less readily, and the saturation coverage diminishes from 0.75 ML at 225 K to 0.65 at 150 K, in agreement with experimental results.[3] Because of the lateral interactions the threefold and top sites get approximately equal effective adsorption energies during the formation of the (2×2)-3NO structure. This results in a very fast hopping of NO from top sites to neighboring threefold sites and back, until another NO molecule moves in to block diffusion to the threefold site. This forced us to reduce the prefactor for top to threefold and threefold to top diffusion with respect to the prefactor for threefold to threefold diffusion, but tests with equal prefactors showed no noticeable influence on the results.

For a nonzero next-next-nearest-neighbor lateral interaction during adsorption at 0.50 ML large c(4×2)-2NO islands are formed, which hardly reconstruct. This slow conversion of the c(4×2)-2NO islands into the (2×2)-3NO structure is due to several factors. First, the strong next-nearest-neighbor lateral interaction of 26 kJ/mol prevents restructuring from within the islands, so reconstruction has to take place at the edges of the islands. Another factor may be that reconstruction occurs through bridge sites, which were not explicitly incorporated in our model. Last, the effective adsorption rate is in reality higher than in our model because of precursor adsorption behavior. Tests with increased adsorption rates and/or defects in the c(4×2)-2NO adlayer give, as expected, a faster conversion into the (2×2)-3NO structure. Increasing the coverage above 0.75 ML causes adsorbates to occupy next-nearest-neighbor positions. Since the repulsion between two next-nearest-neighbor NO molecules is relatively strong (26 kJ/mol), 0.75 ML is the saturation coverage at low temperatures and under UHV conditions. Under high pressures and higher temperatures, however, another ordered structure for NO on Rh(111) was recently discovered with a slightly higher coverage (0.778 ML). This structure does involve next-nearest-neighbor lateral interactions between the adsorbates, but these are compensated by having less adsorbates in the high-energy top sites, resulting in comparable energies for both structures.[33] It is interesting to note that with only minor changes in lateral interactions we could also reproduce this structure. In this paper we restrict ourselves to coverages up to 0.75 ML, however.

C. Temperature programmed desorption

1. Single-site model

We first performed simulations with the single-site model,[20,21] which was very well able to reproduce the TPD spectra, but, since it was only a single-site model, could not reproduce the correct spatial ordering of adsorbates on the surface. Adsorbates in this model occupy neighboring sites at higher coverages, i.e., sites one lattice vector apart. We show here examples at two different coverages, 0.50 and 0.75 ML (Fig. 5). At 0.50 ML, each NO has two neighbors at one lattice vector distance, while in the three-site model and in the experiment it is found that each NO has two neighbors at a larger distance, $2/\sqrt{3}$ lattice vectors apart. At a coverage of 0.75 ML, the number of neighbors at one lattice vector distance even increases to four. In the three-site model and the experiment on the other hand, the number of neighboring NO molecules increases to six, but they are still separated $2/\sqrt{3}$ lattice vectors from each other.

Since large lateral interactions at nearest-neighbor distance in the single-site model caused blocked adsorption and premature desorption (i.e., at lower temperatures), the interactions had to be decreased to much lower values in order to reproduce the TPD spectra. The lateral interactions in that

TABLE VI. Lateral interactions for NO on Rh(111) (kJ/mol) at 1 $d_{\text{Rh-Rh}}$ (nearest neighbor) in the single-site model. Since the interactions are pairwise, the lower left part of the table is identical to the upper right part. We have therefore only reported the lower left part.

	NO threefold		
NO threefold	0	N threefold	
N threefold	12.5	8	O threefold
O threefold	12.5	0	2

model (Table VI) were therefore at odds with results obtained from our (Table V) and Loffreda *et al.*'s[30] DFT calculations.

2. Three-site model

This discrepancy between the actual lateral interactions and adsorbate distribution and the ones in our single-site model led us to do simulations on the more elaborate three-site model. In this model the experimentally found ordered structures are reproduced, and the lateral interactions are consistent with the values derived from the DFT calculations. Figure 6 shows a set of simulated TPD spectra, which closely resemble the experimental spectra previously published in Ref. 6 and here reproduced in Fig. 7. The low coverage region (left), with a coverage below 0.20 ML, is characterized by dissociation of all NO. NO occupies threefold sites. Dissociation starts at 275 K, and is complete just above 350 K. Nitrogen formation occurs in a wide second order peak between 450 and 650 K. The dissociation is not hampered by a lack of accessible sites at these coverages, since even after dissociation of all NO the total coverage is only 0.40 ML. No desorption of NO takes place, since dissociation is faster than desorption. We distinguish between free and accessible sites, since even for saturated overlayers there are many non-occupied or free sites, but these are not accessible for molecules to bind to since this would cause a large repulsion with the neighboring adsorbates.

The medium coverage region (between 0.20 and 0.50 ML, center) is characterized by partial decomposition of threefold NO. N and O form islands (local coverage 0.30–0.35 ML, unordered) separated from the NO islands; dissociation stops when the NO islands are compressed into an ordered structure of 0.50 ML coverage. The formation of separate N+O and NO islands can be explained by a closer look at the lateral interactions (Table V). NO adsorbates can be packed together at next-next-nearest-neighbor distance without a penalty, while this is not possible for nitrogen or oxygen adatoms. If the adlayer is therefore allowed to relax, then the adlayer will try to remove most of the interactions, or at least the stronger ones. This is most easily done by compressing the NO islands to a local coverage of 0.50 ML, while leaving the N+O islands untouched. Nitrogen and oxygen both have considerable interactions at next-next-nearest-neighbor distance; they therefore do not approach each other to such close proximity. Only when part of the NO desorbs, above 400 K, can more NO dissociate.

This clearly demonstrates the influence of the lateral interactions: NO dissociation causes an increase in coverage. Because of the increase in coverage, the amount of repulsion increases, and the dissociation becomes more difficult. The dissociation process therefore becomes more and more difficult until it just stops. There are still empty sites present, but the activation energy for dissociation is too high due to all the repulsions. A similar segregation into islands was seen in co-adsorption experiments of NO+N and NO+O by Xu *et al.*[34] Only after the onset of desorption of NO at around 425 K are some more accessible sites (i.e., sites with less neighboring adsorbates) generated, and can dissociation proceed. The result is that (for this coverage of 0.40 ML) 50% of the NO desorbs, and the other 50% dissociates, causing the formation of 0.20 ML N atoms (which readily desorb as N_2) and 0.20 ML of O atoms which stay on the surface. The desorption of nitrogen gas occurs in two peaks, one almost coinciding with the NO desorption peak, the other one much wider and at higher temperatures. This coincidence of the first peak is caused by the fast formation of N atoms on one hand and the repulsive interactions still present at 450 K. After the NO has disappeared there are few interactions, the

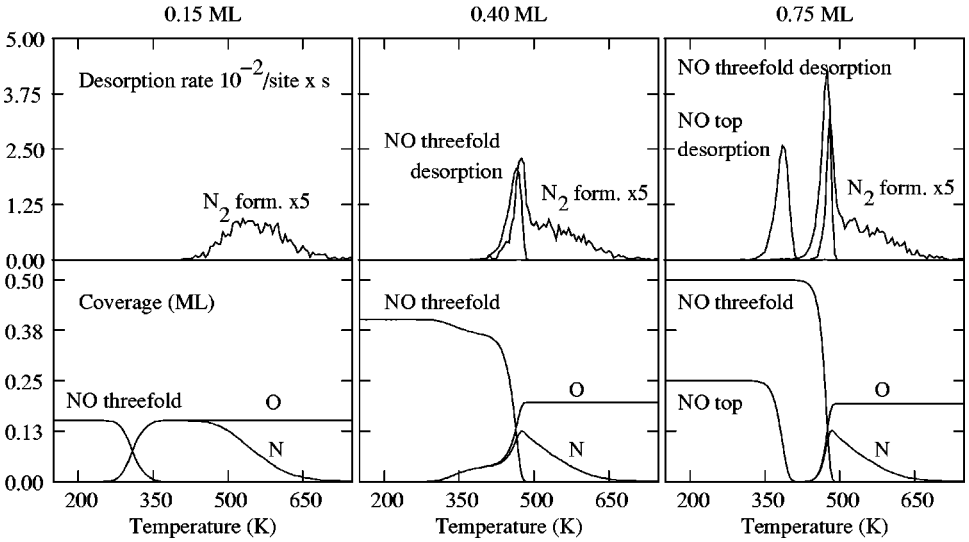

FIG. 6. NO and N_2 desorption rates (top), and NO, nitrogen and oxygen coverages (bottom), during temperature programmed desorption. Starting coverages are (from left panel to right) 0.15, 0.40 and 0.75 ML. N_2 desorption rates have been multiplied by 5; the heating rate was 10 K/s.

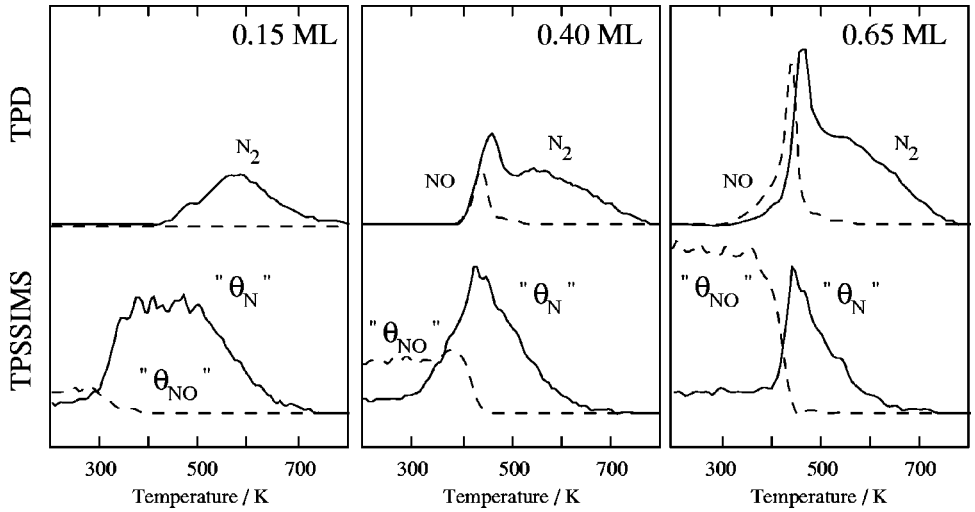

FIG. 7. The NO (- - -) and N_2 (—) TPD rates (top), and $\Sigma_{n=1,2}Rh_nNO^+/Rh_n^+$ (- - -) and Rh_2N^+/Rh_2^+ (—) TPSSIMS ion intensity ratios (bottom), during the temperature programmed reaction of NO on Rh(111) for low (left panel), medium (central panel) and high (right panel) initial NO coverages. The NO TPD spectra have been divided by a factor 4 with respect to the N_2 TPD spectra. The adsorption temperature was 100 K; the heating rate was 10 K/s. Adapted from Ref. 6.

activation energy for nitrogen formation is higher and the remaining N atoms on the surface desorb in a broad peak.

At coverages close to saturation (above 0.50 ML), dissociation is completely inhibited up to 400 K (right). Top bound NO desorbs around 380 K, but does not create the vacancies needed for dissociation. After the desorption of threefold NO above 400 K, dissociation proceeds, and nitrogen formation occurs in a first and a second order peak. This total blockage of dissociation is due to the absence of accessible sites. When the top-bound NO desorbs, top sites are freed, but these are not capable of binding N or O adatoms. Dissociation is therefore suppressed until the desorption of threefold-bound NO. Then dissociation and desorption compete again, with 0.20 ML NO dissociating and the rest desorbing. The amount of NO that dissociates therefore does not increase with NO starting coverage increasing from 0.40 to 0.75 ML. This maximum amount of dissociated NO is directly related to the competition between desorption and dissociation, since it is known that upon re-adsorption of NO higher N+O coverages can be generated. The amount of dissociated and desorbed NO versus initial NO coverage thus shows the following trend: below 0.20 ML initial coverage all NO dissociates, above 0.20 ML initial coverage 0.20 ML NO dissociates and the rest desorbs. Experimentally this was also measured. Borg *et al.*[6] found that for initial coverages up to 0.25 ML all NO dissociates, and that for higher coverages NO both dissociates and desorbs. The amount of dissociated NO increases with the initial NO coverage, even for coverages larger than 0.25 ML. Hardeveld[35] on the other hand found that for initial coverages up to 0.20 ML all NO dissociates. Between 0.20 and 0.45 ML initial coverage 0.20 ML NO dissociates while the rest desorbs. For coverages above 0.45 ML a further increase in the amount of dissociated NO was found while the amount of desorbed NO remained constant. Aryafar *et al.*[19] have also shown that for coverages up to 0.20 ML all NO dissociates with little NO desorption. They found that at higher coverages 0.20 ML NO dissociates, the rest desorbs molecularly.

We conclude by remarking that in order to keep the model more simple, we modeled the dissociation reaction on the terrace, although there is considerable experimental evidence that this in fact occurs at steps in the surface.[16,36,37] In the case that diffusion to the steps is fast, the reaction at the steps can be modeled as a reaction on the terrace with a correction in the prefactor to account for the fraction of active sites. The prefactor for the terrace reaction rate constant then becomes the fraction of steps times the prefactor of the reaction rate constant at the steps. Since diffusion of NO, N and O is fast with respect to the reactions, the condition holds and the macroscopic rates are the same. As for the spatial distribution of adsorbates, it is expected that a similar segregation into separate N+O and NO islands will be seen for the step-reaction, since also in this case the empty sites on the surface will be filled causing compression of the adlayer. A similar suppression of dissociation will be caused by the lack of empty terrace sites, and the fractions of desorbed and dissociated NO will therefore also be comparable. Thus we conclude that despite the omission of steps in our model, the simulations presented here are able to describe the most important experimental features.

IV. CONCLUSIONS

We have successfully reproduced the ordering behavior of NO on Rh(111) during adsorption and the temperature programmed desorption (TPD) of NO from Rh(111) under UHV conditions using a dynamic Monte-Carlo model involving lateral interactions derived from DFT calculations and different adsorption sites (top, fcc and hcp). The formation of c(4×2)-2NO domains at 0.50 ML coverage depends strongly on the next-next-nearest-neighbor repulsion between the NO adsorbates used in the model. The formation of the (2×2)-3NO structure at higher coverage follows from the avoidance of the strong next-nearest-neighbor repulsion in favor of the occupation of the top sites.

A single-site model was able to reproduce the experimental TPD, but the lateral interactions were at odds with the values of the DFT calculations. A three-site model resolved this problem. All NO dissociates during TPD for initial coverages of NO below 0.20 ML. For NO coverages larger than 0.20 ML, 0.20 ML NO dissociates while the rest desorbs. This is due to a lack of accessible sites on the surface, i.e.,

sites where a molecule can bind without experiencing large repulsions with neighboring adsorbates. For NO coverages above 0.20 ML, the dissociation of NO causes a segregation into separate NO and N+O islands. The dissociation causes the surface to be filled with adsorbates, and the adsorbates are therefore pushed closer together. NO on one hand can easily be compressed into islands of 0.50 ML coverage, because there is no large next-next-nearest-neighbor repulsion. N+O on the other hand form islands with a lower coverage (0.30–0.35 ML) due to the considerable next-next-nearest-neighbor repulsion. Top bound NO (above 0.50 ML initial coverage) does not contribute to the amount of NO dissociated during TPD, it desorbs in a separate peak at 380 K. Instead, dissociation is blocked until the desorption of threefold bound NO.

We would like to acknowledge many interesting and fruitful discussions with Dr. M. T. M. Koper and with Professor P. A. J. Hilbers (all of the Eindhoven University of Technology) and Professor P. Sautet and Dr. D. Loffreda of the Institut de Recherches sur la Catalyse, Villeurbane. Financial support by the NRSC-Catalysis is gratefully acknowledged.

[1] C.-T. Kao, G. S. Blackman, M. A. van Hove, and G. A. Somorjai, Surf. Sci. **224**, 77 (1989).
[2] I. Zasada, M. A. van Hove, and G. A. Somorjai, Surf. Sci. **418**, L89 (1998).
[3] T. W. Root, L. D. Schmidt, and G. B. Fisher, Surf. Sci. **134**, 30 (1983).
[4] N. Materer, A. Barbieri, D. Gardin, U. Starke, J. D. Batteas, and M. A. van Hove, Surf. Sci. **303**, 319 (1994).
[5] M. Stichler and D. Menzel, Surf. Sci. **391**, 47 (1997).
[6] H. J. Borg, J. F. C.-J. Reijerse, R. A. van Santen, and J. W. Niemantsverdriet, J. Chem. Phys. **101**, 10052 (1994).
[7] J. J. Lukkien, J. P. L. Segers, P. A. J. Hilbers, R. J. Gelten, and A. P. J. Jansen, Phys. Rev. E **58**, 2598 (1998).
[8] A. P. J. Jansen, Comput. Phys. Commun. **86**, 1 (1995).
[9] CARLOS is a general-purpose program, written in C, for simulating reactions on surfaces that can be represented by regular grids; an implementation of the First-Reaction Method and the Variable Stepsize Method, written by J. J. Lukkien.
[10] R. J. Gelten, R. A. van Santen, and A. P. J. Jansen, *Molecular dynamics. From Classical to Quantum Methods* (Elsevier Science B.V., 1999), Vol. 7 of *Theoretical and Computational Chemistry*, Chap. Dynamic Monte Carlo Simulations of Oscillatory Heterogeneous Catalytic Reactions, pp. 737–784.
[11] N. G. van Kampen, Ed., *Stochastic Processes in Physics and Chemistry* (North-Holland, Amsterdam, 1992).
[12] M. G. Evans and M. Polanyi, Trans. Faraday Soc. **34**, 11 (1938).
[13] J. N. Brönsted, Chem. Rev. **5**, 231 (1928).
[14] R. I. Masel, Ed., *Principles of Adsorption and Reaction on Solid Surfaces*, Wiley series in chemical engineering (Wiley, New York, 1996).
[15] G. Ertl, H. Knoezinger, and J. Weitkamp, Eds., *Handbook of Heterogeneous Catalysis*, Vol. 3 (Weinheim, New York, 1997).
[16] L. A. DeLouise and N. Winograd, Surf. Sci. **159**, 199 (1985).
[17] T. W. Root, G. B. Fisher, and L. D. Schmidt, J. Chem. Phys. **85**, 4679 (1986).
[18] Y. J. Kim, S. Thevuthasan, G. S. Herman, C. H. F. Peden, S. A. Chambers, D. N. Belton, and H. Permana, Surf. Sci. **359**, 269 (1996).
[19] M. Aryafar and F. Zaera, J. Catal. **175**, 316 (1998).
[20] R. M. van Hardeveld, M. J. P. Hopstaken, J. J. Lukkien, P. A. J. Hilbers, A. P. J. Jansen, R. A. van Santen, and J. W. Niemantsverdriet, Chem. Phys. Lett. **302**, 98 (1999).
[21] R. M. Nieminen and A. P. J. Jansen, Appl. Catal., A **160**, 99 (1997).
[22] E. W. Hansen and M. Neurock, Surf. Sci. **464**, 91 (2000).
[23] K. Honkala, P. Pirilä, and K. Laasonen, Phys. Rev. Lett. **86**, 5942 (2001).
[24] C. Stampfl, H. J. Kreuzer, S. H. Payne, H. Pfnür, and M. Scheffler, Phys. Rev. Lett. **83**, 2993 (1999).
[25] G. Kresse and J. Furthmüller, Comput. Mater. Sci. **6**, 15 (1996).
[26] G. Kresse and J. Furthmüller, Phys. Rev. B **54**, 11169 (1996).
[27] J. P. Perdew, *Electronic Structure of Solids '91* (Akademie Verlag, Berlin, 1991).
[28] D. Vanderbilt, Phys. Rev. B **41**, 7892 (1990).
[29] G. Kresse and J. Hafner, J. Phys.: Condens. Matter **6**, 8245 (1994).
[30] D. Loffreda, D. Simon, and P. Sautet, J. Chem. Phys. **108**, 6447 (1998).
[31] Q. Ge, R. Kose, and D. A. King, Adv. Catal. **45**, 207 (2000).
[32] D. Loffreda, Ph.D. thesis, Université Claude Bernard-Lyon 1 (1999).
[33] K. B. Rider, K. S. Hwang, M. Salmeron, and G. A. Somorjai, Phys. Rev. Lett. **86**, 4330 (2001).
[34] H. Xu and K. Y. S. Ng, Surf. Sci. **365**, 779 (1996).
[35] M. van Hardeveld, Ph.D. thesis, Eindhoven University of Technology (1997).
[36] N. M. H. Janssen, A. R. Colach, M. Ikai, K. Tanaka, and B. E. Nieuwenhuys, Surf. Sci. **382**, 201 (1997).
[37] F. Esch, A. Baraldi, C. Comelli, S. Lizzit, M. Kiskinova, P. D. Cobden, and B. E. Nieuwenhuys, J. Chem. Phys. **110**, 4013 (1999).